

Article

Application of Mineral Iron-Based Natural Catalysts in Electro-Fenton Process: A Comparative Study

Zahra Heidari ¹, Rasool Pelalak ^{1,2,3}, Reza Alizadeh ^{4,*}, Nihal Oturan ¹, Saeed Shirazian ^{2,3,5} 
and Mehmet A. Oturan ^{1,*}

¹ IFSA, Laboratoire Géomatériaux et Environnement (LGE), Université Gustave Eiffel, 5, Boulevard Descartes, Champs sur Marne, 77454 Marne-la-Vallée, France; Z_heidari@sut.ac.ir (Z.H.); rasoolpelalak@duytan.edu.vn (R.P.); nihal.oturan@u-pem.fr (N.O.)

² Institute of Research and Development, Duy Tan University, Da Nang 550000, Vietnam; Saeed.Shirazian@ul.ie

³ Faculty of Environmental and Chemical Engineering, Duy Tan University, Da Nang 550000, Vietnam

⁴ Chemical Engineering Faculty, Sahand University of Technology, Sahand New Town, Tabriz P.O. Box 51335-1996, Iran

⁵ Laboratory of Computational Modeling of Drugs, South Ural State University, 76 Lenin prospekt, 454080 Chelyabinsk, Russia

* Correspondence: r.alizadeh@sut.ac.ir (R.A.); mehmet.oturan@univ-eiffel.fr (M.A.O.)

Abstract: The potential use of novel iron based mineral catalysts as an effective and available material for electrocatalytic oxidation of refractory contaminants by heterogeneous electro-Fenton (HEF) process was studied for the first time. For this purpose, four natural catalysts, namely ilmenite (FeTiO₃), pyrite (FeS₂), chromite (FeCr₂O₄), and chalcopyrite (CuFeS₂) were selected as the source of ferrous iron (Fe²⁺) ions. The catalyst samples were appropriately characterized by X-ray diffraction (XRD) and RAMAN analysis. The degradation kinetics and mineralization rate of 0.2 mM antibiotic cefazolin (CFZ), as a contaminant of emerging concern, were comparatively investigated by HEF using the catalysts mentioned above. The effect of important experimental parameters such as catalysts loading and current on the process efficiency was investigated. Moreover, the performance of these new mineral catalysts was compared in term of CFZ degradation kinetics, mineralization power, mineralization current efficiency and electrical energy consumption. A greater enhancement in degradation/mineralization of CFZ was obtained when using chalcopyrite as the catalyst in HEF. The stability and reusability experiments demonstrated negligible decrease in catalytic activity of chalcopyrite after five consecutive runs. Besides, the rate constant for CFZ oxidation by hydroxyl radicals was estimated according the pseudo-first-order reaction kinetics. The empirical assessment, in addition to economic evaluation, confirmed that iron based mineral catalysts and specifically chalcopyrite could be an appropriate and cost-effective alternative catalyst for HEF due to its high catalytic activity, availability, eco-friendly nature and low energy consumption compared to other synthesized catalysts.

Keywords: iron based mineral catalysts; electrochemical advanced oxidation; mineralization; cefazolin; wastewater treatment



Citation: Heidari, Z.; Pelalak, R.; Alizadeh, R.; Oturan, N.; Shirazian, S.; Oturan, M.A. Application of Mineral Iron-Based Natural Catalysts in Electro-Fenton Process: A Comparative Study. *Catalysts* **2021**, *11*, 57.

<https://doi.org/10.3390/catal11010057>

Received: 7 December 2020

Accepted: 30 December 2020

Published: 2 January 2021

Publisher's Note: MDPI stays neutral with regard to jurisdictional claims in published maps and institutional affiliations.



Copyright: © 2021 by the authors. Licensee MDPI, Basel, Switzerland. This article is an open access article distributed under the terms and conditions of the Creative Commons Attribution (CC BY) license (<https://creativecommons.org/licenses/by/4.0/>).

1. Introduction

Pharmaceuticals, and especially antibiotics, in surface and ground water have extensively received attention due to their toxic potential and serious risk to human and living organisms due to antibiotic resistance, endocrine disruption, allergic reactions and cancer [1–5]. It has been reported that the major part of these pharmaceuticals could have been discharged from pharmaceutical industries, hospital effluents and direct disposal of unused drugs in wastewater [6–8]. Cefazolin (CFZ) is an antibiotic prescribed for the treatment of several bacterial diseases in the stomach, lung, bones, joints, and urinary tract [9,10]. It is present in surface and ground water in the range of ng L⁻¹ to µg L⁻¹ [11–13]. The presence

of pharmaceuticals in effluents is mainly the result of ineffective removal technologies used in conventional wastewater treatment plants [14–16].

Different treatment methods have been used to remove organic pollutants from wastewater such as adsorption [17–21], membrane processes [22,23], biological methods [24,25] and advanced oxidation processes (AOPs) [26–29]. During recent decades, AOPs confirmed their effective degradation ability due to the production of powerful reactive oxidants [30–33]. Among different AOPs electrochemical advanced oxidation processes (EAOPs) have proved their ability for effective and fast degradation of refractory, toxic and non-biodegradable organic contaminants [4,34,35]. In addition, these processes have significant advantages such as low operational cost, eco-friendly nature, high pollutant mineralization power, and operation under mild conditions (temperature and pressure) [36,37]. The Electro-Fenton (EF) process is one of the most powerful and attractive EAOPs. The mechanism of this process is based on the in-situ generation of hydroxyl radicals ($\bullet\text{OH}$) from electrochemically formed H_2O_2 (Equation. (1)) when using a carbonaceous cathode (such as carbon or graphite felt, carbon nanotubes, carbon sponge) in presence of the externally added ferrous ions as catalyst. H_2O_2 thus formed reacts with Fe^{2+} ion according to the Fenton reaction (Equation. (2)) to generate the highly oxidizing agent $\bullet\text{OH}$. The catalyst (Fe^{2+}) is then electrochemically regenerated (Equation. (3)) to promote continuous production of $\bullet\text{OH}$ in the solution [36,38,39].



Moreover, the use of a high oxygen-overpotential anode like boron doped diamond (BDD) allows the generation of heterogeneous hydroxyl radicals according to Equation (4). The BDD electrode is known as the most powerful and effective anode material for electrochemical applications. In comparison to other anode materials such as DSA, Pt and SnO_2 , the BDD anode can produce more physisorbed $\bullet\text{OH}$ ($\text{BDD}(\bullet\text{OH})$) and a higher oxidation rate is estimated [40–43]. As a result, more hydroxyl radicals are produced in the system leading to the oxidation degradation rate of organic pollutants and effective mineralization of treated solutions.



EF process can be classified as homogeneous or heterogeneous according to the nature of the catalyst used. In contrast to the classical EF using a soluble iron salt, the heterogeneous EF (HEF) process is based on the use of an iron containing solid catalysts [3,44]. The HEF presents advantages such as the easy separation and reusability of the catalyst (avoiding a secondary pollution) and a wide pH range on working [45,46]. Among various types of solid catalysts, natural iron-based materials have attracted researcher's attention due to availability, low cost, non-toxicity, high catalytic activity and ease of separation [47,48]. In this regard, natural catalysts containing iron such as pyrite (FeS_2), bornite (Cu_5FeS_4), magnetite (Fe_2O_3) and wustite (FeO) have been stated as effective natural catalysts in HEF [38,39,48–50]. Ilmenite (FeTiO_3), chromite (FeCr_2O_4), pyrite (FeS_2) and chalcopyrite (CuFeS_2) are green, cheap and available natural iron-based materials which can offer Fe^{2+} ions for employment in HEF [38,51–53].

To study the potential of these natural iron-based catalysts, we have performed an investigation on the degradation/mineralization of the antibiotic CFZ as target contaminant by HEF. In order to obtain the catalytic efficiency of each catalyst, comparative CFZ degradation trials were done under the same operating conditions. Moreover, the effect of current on the CFZ degradation efficiency, mineralization rate, mineralization current efficiency (MCE) and specific energy consumption (SEC) were investigated. Optimum dosage of catalysts was assessed during CFZ degradation. Furthermore, the reusability

tests in five consecutive runs were studied to evaluate the ability of the catalyst for practical wastewater applications. In short, in this study, comparative experiments were performed to highlight the capacity of mineral iron-based catalysts as a promising candidate for HEF.

2. Results and Discussion

2.1. Characterization of Mineral Iron based Catalysts

X-ray diffraction analysis (XRD) was performed to recognize the structure of catalysts and confirm their crystalline structure. XRD analysis was carried out for ilmenite (FeTiO_3), chromite (FeCr_2O_4), pyrite (FeS_2) and chalcopyrite (CuFeS_2) samples and the outcomes presented in Figure 1. In comparison with Joint Committee on Powder Diffraction Standards (JCPDS) data, the main peak positions in Figure 1a are in good agreement with characteristic peaks of ilmenite at about 24.1, 27.7, 32.9, 35.6, 40.6, 44.5, 49.1, 53.4, 56.6, 61.9, 63.7, 70.5 and 74.8 (JCPDS No 98-001-7090). The XRD peaks of pyrite (Figure 1b) were found to correspond well with the characteristic peaks of pyrite at 2θ values of 25.5, 26.9, 32.3, 33.3, 37, 40.9, 47.7, 56.5, 59.5, 64.3 and 68.2 (JCPDC No of 98-008-1773). Furthermore, the index peaks presented in Figure 1c were in accordance with standard JCPDS references of chromite (JCPDS No 98-004-8655). Finally, according to the patterns in Figure 1d, it was demonstrated that the peaks located at 2θ values of 29.7, 34.4, 49.2, and 58.3 are in agreement with the characteristic peaks reported for chalcopyrite (JCPDC No of 00-001-0842). The high intensity of parasitic peaks related to impurities were not found in any iron-based catalysts, which make it possible to conclude that all titled catalysts are mainly pure.

Raman spectroscopy analysis can be used to explore the vibrations and features of crystal structures of materials [54]. The Raman spectra of ilmenite, pyrite, chalcopyrite and chromite catalysts are shown in Figure 2. In the Raman spectra of ilmenite sample (Figure 2a), the results indicated the presence of peaks at 240, 373, and 689 cm^{-1} related to the FeTiO_3 [55]. Figure 2b showed the Raman spectrum of pyrite comprising three sharp peaks between 200 cm^{-1} and 500 cm^{-1} (343 , 380 , and 430 cm^{-1}) and their positions agree with those reported for FeS_2 [56]. The bands at $400\text{--}800\text{ cm}^{-1}$ in Figure 2c with two peaks at around 557 cm^{-1} and 693 cm^{-1} are attributed to chromite on the basis of previous Raman studies [57]. The chalcopyrite samples (Figure 2d) displayed four characteristic peaks at 290, 317, 350, and 470 cm^{-1} in accordance with Yang et al. [58]. Therefore, it can be concluded that the Raman analysis confirmed the nature of all mentioned catalysts.

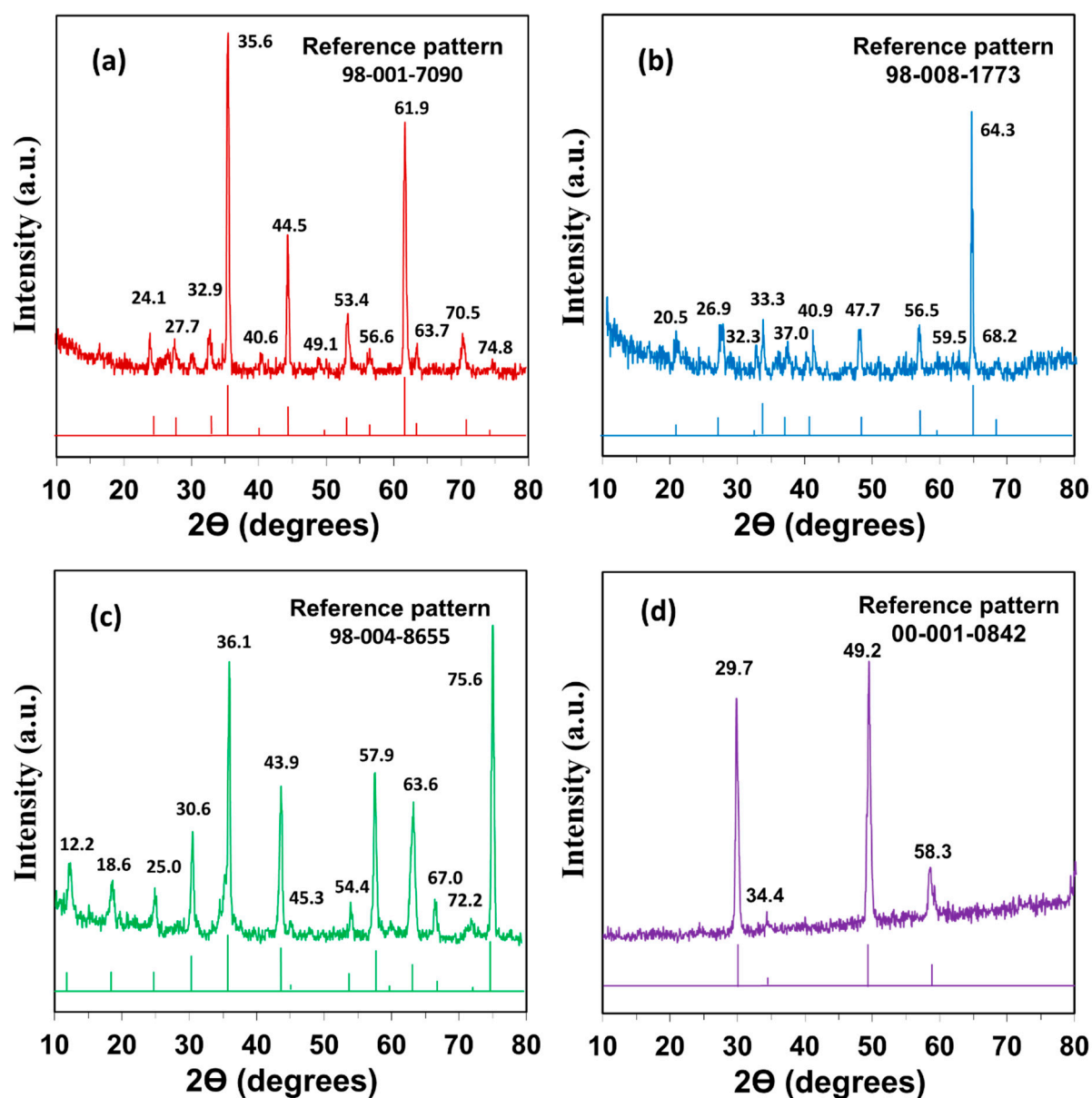


Figure 1. X-ray diffraction (XRD) patterns of mineral iron-based catalysts: (a) ilmenite, (b) pyrite, (c) chromite, and (d) chalcopyrite.

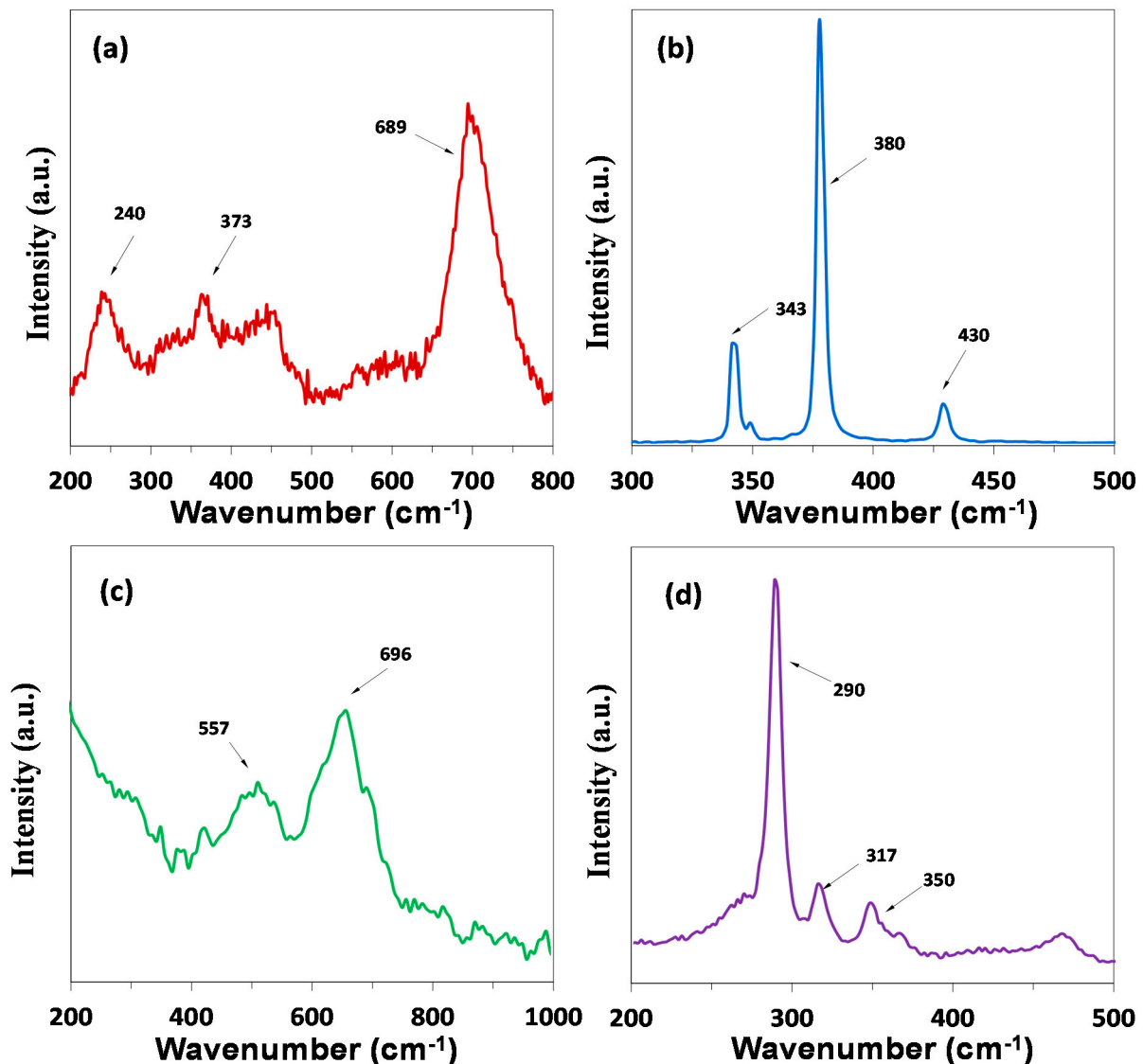


Figure 2. Raman analysis of mineral iron-based catalysts: (a) ilmenite, (b) pyrite, (c) chromite, and (d) chalcopyrite.

2.2. Effect of Operating Parameter on CFZ Decay Kinetics during HEF

Among the influential parameters in HEF, the applied current and the catalyst dosage constitute the most important. Therefore, the effect of these two parameters on the oxidative degradation of CFZ was investigated.

2.2.1. Effect of Applied Current

The applied current constitutes a significant operating variable in HEF, which considerably affects the process efficiency and the operating costs. Indeed, this parameter controls the $\bullet\text{OH}$ generation rate in the bulk solution according to the Equations (1)–(3) and on the anode surface (Equation. 4), and hence strongly affect the abatement of contaminants. Thus, the effect of applied current on the CFZ degradation kinetics during HEF with different mineral iron-based catalysts, namely, ilmenite, chromite, pyrite and chalcopyrite, was investigated. The comparative studies were done for 0.20 mM CFZ concentration in 230 mL solution of 0.050 M Na_2SO_4 with 1 g L^{-1} dosage of different catalysts in a BDD/carbon felt cell at currents ranging between 50 and 500 mA and results are shown in Figure 3. As can be seen, a complete abatement of CFZ concentration was obtained for all currents and mineral catalysts under the same operating conditions. Low

currents required about 40 min to reach complete depletion of CFZ (except the ilmenite requiring a longer electrolysis time than 40 min). Oxidative degradation kinetics of CFZ concentration decay are enhanced by increasing the applied current value, and complete disappearance of CFZ was attained at 500 mA with all catalysts. On the other hand, the degradation kinetics curves are close for the currents from 200 to 500 mA (Figure 3a–d). As high currents cause high-energy consumption, a current of 200 mA was kept as optimum value. When comparing the results at 200 mA, it can be seen that the chalcopyrite provides a higher $\bullet\text{OH}$ production ability than the others in the degradation of CFZ during HEF. The complete depletion of CFZ takes place in 15 min, while it requires 20 min with others. This can be explained by the intrinsic property of chalcopyrite, which releases Cu^{2+} ions in addition to Fe^{2+} ions into the reaction medium. Cu^{2+} ions behave as catalyst like Fe^{2+} ions to catalyze H_2O_2 decomposition and generate $\bullet\text{OH}$ according to Equations (5)–(8). First, Cu^{2+} ions can be reduced to Cu^+ ions in the bulk of solution according to Equations (5) and (6), or at the carbon felt cathode (Equation (7)). Then the produced Cu^+ ions can react with H_2O_2 according to the Fenton-like reaction and produce $\bullet\text{OH}$ (Equation (8)). In addition, it is worthy to note that Cu^+ ions can also regenerate Fe^{2+} ions and consequently enhance the Fenton reaction (Equation (9)) [36,52,59].

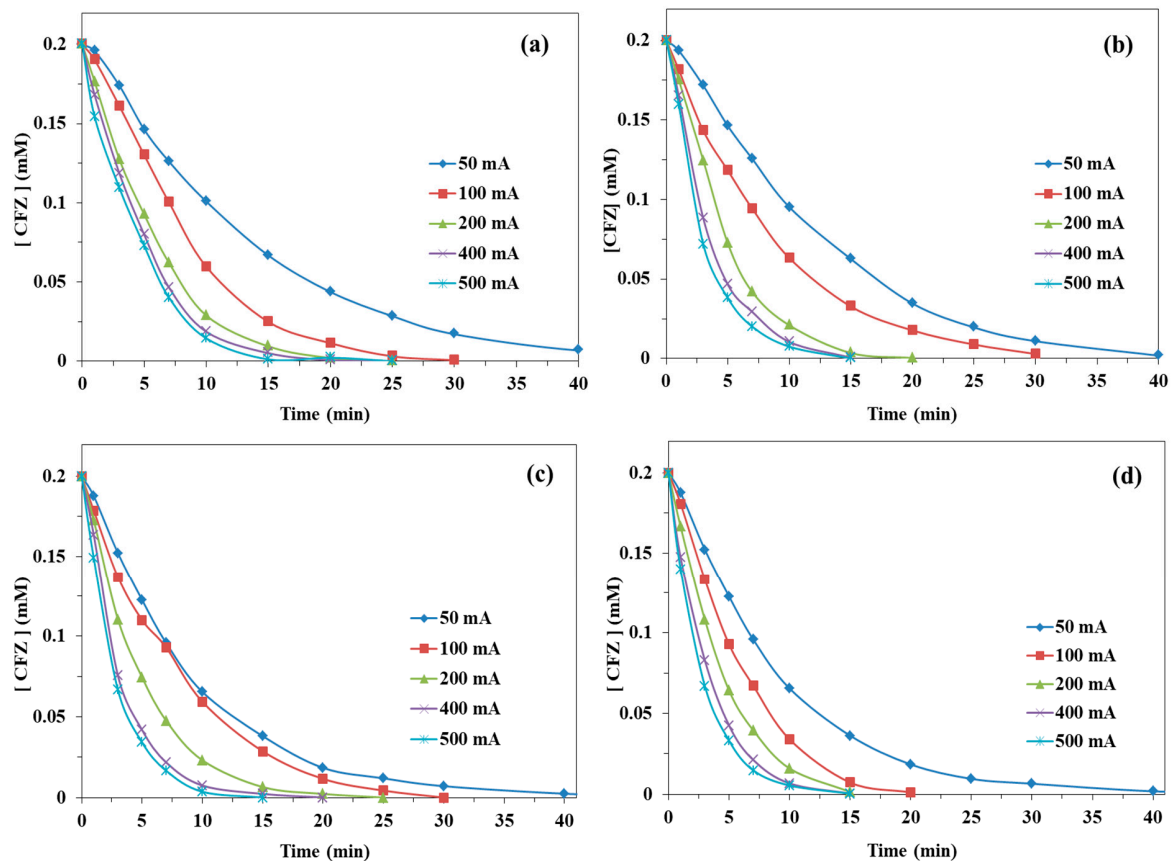
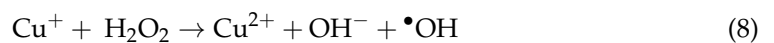
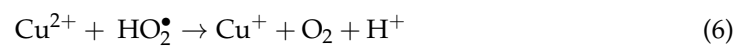
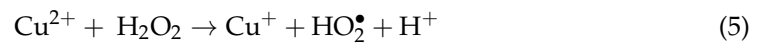


Figure 3. Effect of applied current on the cefazolin (CFZ) degradation with HEFPs using different mineral iron-based catalysts: (a) ilmenite, (b) pyrite, (c) chromite, and (d) chalcopyrite.

2.2.2. Effect of Catalyst Dosage

The catalyst loading has a significant impact on the efficiency of HEFPs. To investigate the effect of ilmenite, pyrite, chalcopyrite and chromite loading on CFZ degradation several tests were performed at 100 mA and 230 mL of 0.20 mM CFZ. The HEFPs were performed with a BDD anode and carbon felt cathode while the catalyst dosage was varied in the range of 0.5–2.0 g L⁻¹. The results of these experiments which are depicted in Figure 4a–d show that, by using the lowest amount of pyrite, chromite, and ilmenite catalysts, the complete degradation of CFZ was attained in 40 min of reaction, while in the case of chalcopyrite CFZ totally degraded at a slightly shorter time of HEFP (30 min). A quick decay of CFZ concentration happened by increasing the catalysts, loading from 0.5 g L⁻¹ to 1 g L⁻¹ for all named catalysts. This increase could be due to the enhancement in Fe²⁺ release from the surface of iron-based catalysts which consequently produce more •OH in HEFPs by increasing the catalytic loading. On the contrary, CFZ degradation was decreased by further increase in catalyst loading (up to 2.0 g L⁻¹). The reason for this decrease can be due to the participation of excess Fe²⁺ ions in the wasting reactions (Equation (10)). Parallel consumption •OH by reacting with Fe²⁺ ions inhibits the oxidation of CFZ by •OH and in this way decreases CFZ degradation.

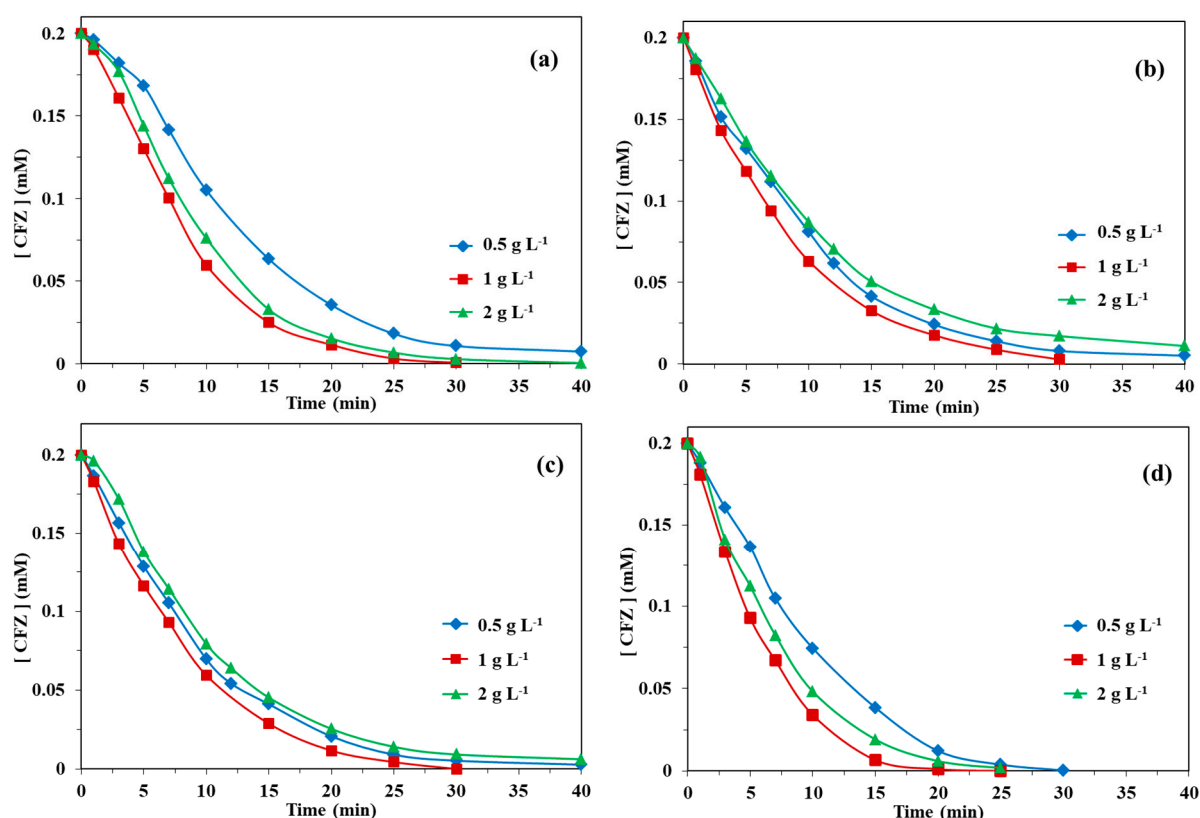


Figure 4. Effect of catalysts loading on the CFZ degradation with HEFPs at 100 mA using different mineral iron-based catalysts: (a) ilmenite, (b) pyrite, (c) chromite, and (d) chalcopyrite.

Consequently, the 1 g L⁻¹ of all mentioned catalysts seems to be the most effective amount of for degradation of CFZ antibiotic and the remaining tests were performed with this amount.

2.3. Mineralization of CFZ during HEFPs

In order to assess the iron-based catalytic oxidation of CFZ and its removal from water, it is essential to investigate the total organic carbon (TOC) decay analysis of the solution during HEF experiments. To assess the mineralization ability of different catalysts, the TOC removal of CFZ (0.2 mM) against reaction time was studied as a function of the applied current. Samples were collected during HEF treatment using ilmenite, pyrite, chromite, and chalcopyrite as catalysts in a BDD/carbon felt cell. As can be seen from Figure 5, TOC removal always gradually reduced with electrolysis time. Besides, the TOC removal rate of CFZ solution increased when raising the value of current in accordance with the trend noticed in CFZ oxidation, due to the higher $\bullet\text{OH}$ production (in bulk solution and on the BDD surface) at higher applied current values, as explained in the previous sub-section. The higher amount of produced $\bullet\text{OH}$ can oxidize CFZ and its byproducts more quickly. Higher currents (400 and 500 mA) lead to a mineralization rate of more than 90% after 6 h of experiments. As mentioned, when using chalcopyrite as catalyst, almost complete mineralization was reached at 8 h electrolysis. A TOC removal rate of about 94% was obtained with other catalysts (ilmenite, pyrite and chromite) with a difference lower than 1% at 500 mA and 8 h. This means that ilmenite, pyrite and chromite have almost the same mineralization ability. At such a mineralization rate, the remaining TOC is composed of residual short-chain carboxylic acids.

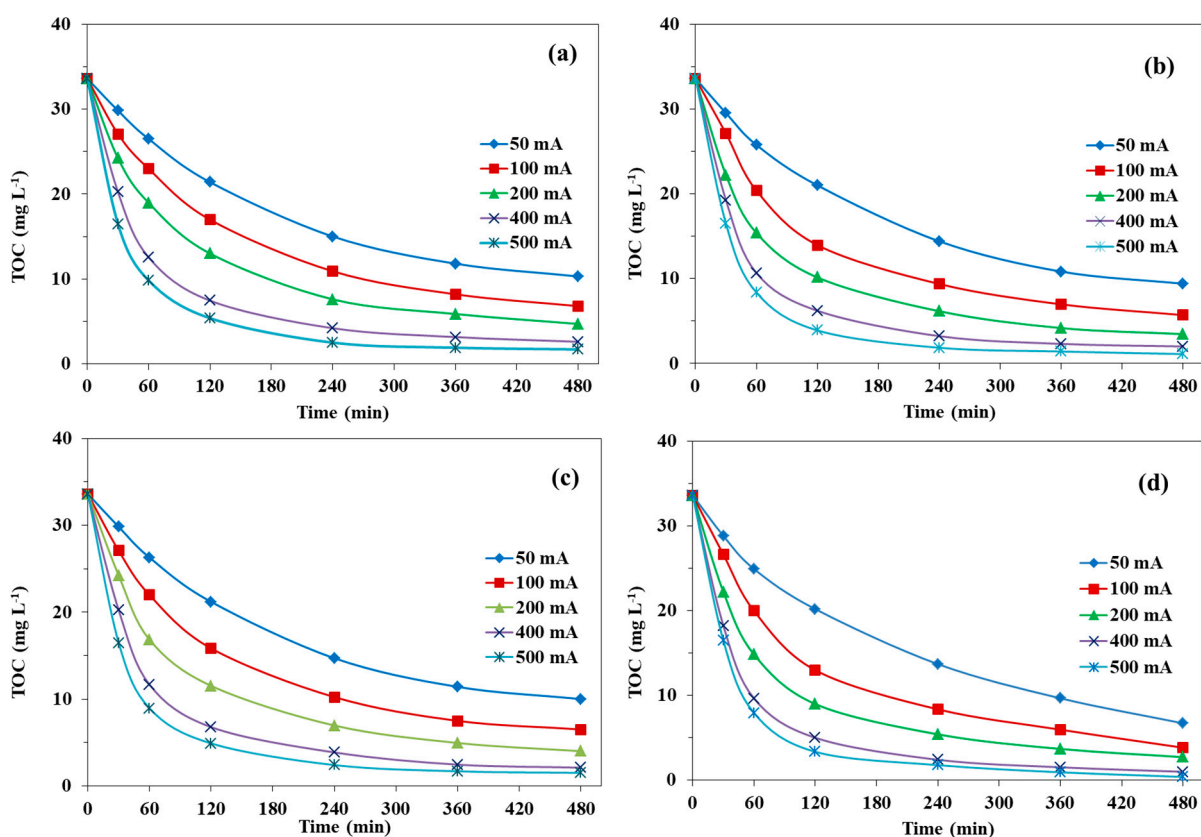


Figure 5. Effect of applied current on the mineralization kinetics of 0.2 mM CFZ solution (corresponding to total organic carbon $(\text{TOC})_0 = 33.6 \text{ mg L}^{-1}$ of carbon) by HEF using different mineral iron-based catalysts: (a) ilmenite, (b) pyrite, (c) chromite, and (d) chalcopyrite.

2.4. Kinetics of CFZ Degradation by HEF

The degradation kinetics of 0.2 mM CFZ in HEF using different natural catalysts was studied under the same operating condition. The current applied to the electrolytic cell being constant, $\bullet\text{OH}$ are produced at a constant rate in the system. As $\bullet\text{OH}$ are a very

reactive species, they are consumed as soon as they are produced. Therefore, the steady state assumption can be applied to the concentration of $\bullet\text{OH}$. In this case, the second order reaction kinetics of CFZ can be written as follows:



$$\frac{d[\text{CFZ}]}{dt} = -k [\text{CFZ}][\text{HO}\bullet] = -k_{\text{abs}} [\text{CFZ}] \quad (12)$$

where $k_{\text{app}} = \text{apparent rate constant} = k [\bullet\text{OH}] = \text{constant}$. Thus, under these conditions, the second order reaction becomes a pseudo first-order reaction. The integration of Equation (12) gives the following Equation (13):

$$\text{Ln} [\text{CFZ}]_t = \text{Ln} [\text{CFZ}]_0 - k_{\text{app}} \times t \quad (13)$$

Then, k_{app} for oxidative degradation of CFZ can be obtained from Equation (17) by plotting $\text{Ln}([\text{CFZ}]_0/[\text{CFZ}]_t)$ versus t . The slope of straight line allows the value of k_{app} [38,39,46,52] and results obtained are gathered in Table 1 with linear regression coefficients (R^2) for CFZ degradation by HEF using different iron-containing mineral-based catalysts. According to the high values of R^2 obtained in all the trials, it can be concluded that the pseudo-first order kinetics model for oxidation of CFZ by HEF is satisfactorily described.

Table 1. Apparent rate constants for HEFPs using different mineral iron-based catalysts. ($(\text{CFZ})_0 = 0.2 \text{ mM}$).

Parameters.	I (mA)	k_{app} (min^{-1})	R^2
Chalcopyrite	50	0.111	0.994
	100	0.196	0.957
	200	0.241	0.991
	400	0.329	0.995
	500	0.368	0.999
Pyrite	50	0.074	0.986
	100	0.117	0.995
	200	0.219	0.986
	400	0.285	0.992
	500	0.331	0.997
Chromite	50	0.109	0.995
	100	0.123	0.99
	200	0.209	0.996
	400	0.323	0.997
	500	0.355	0.999
Ilmenite	50	0.069	0.987
	100	0.125	0.956
	200	0.179	0.979
	400	0.219	0.977
	500	0.221	0.989

The determined k_{app} values in Table 1 indicate that, in all currents applied in HEF, the chalcopyrite had the highest k_{app} values compared to other catalysts. This result can be explained by the presence of double catalyst ions (Fe^{2+} and Cu^+) in the structure of chalcopyrite, allowing the production of higher amounts of $\bullet\text{OH}$, as mentioned in Section 2.2. Overall, it can be said that the apparent rate constants of CFZ degradation by $\bullet\text{OH}$ in HEF decrease in the following order: chalcopyrite > chromite > pyrite > ilmenite, although the difference between the three last is very small.

2.5. Mineralization Current Efficiency (MCE) and Specific Energy Consumption (SEC)

The MCE% during electrolysis of 0.2 mM CFZ solution (corresponding to 33.6 mg L⁻¹ initial TOC) by HEF with different iron-based catalysts in 8 h was evaluated and the results are depicted in Figure 6. The MCE% values are meaningfully higher at 50 mA compared to other current values with all catalysts. Maximum MCE% is attained at about 29.2%, 32.2%, 30.0% and 35.7% when using ilmenite, pyrite, chromite and chalcopyrite catalysts, respectively, in the first hour of processing. A slightly greater MCE% was found for chalcopyrite compared to other catalysts, in agreement with oxidation and mineralization experiments. Chromite follows chalcopyrite, presenting slightly better efficiency for all currents.

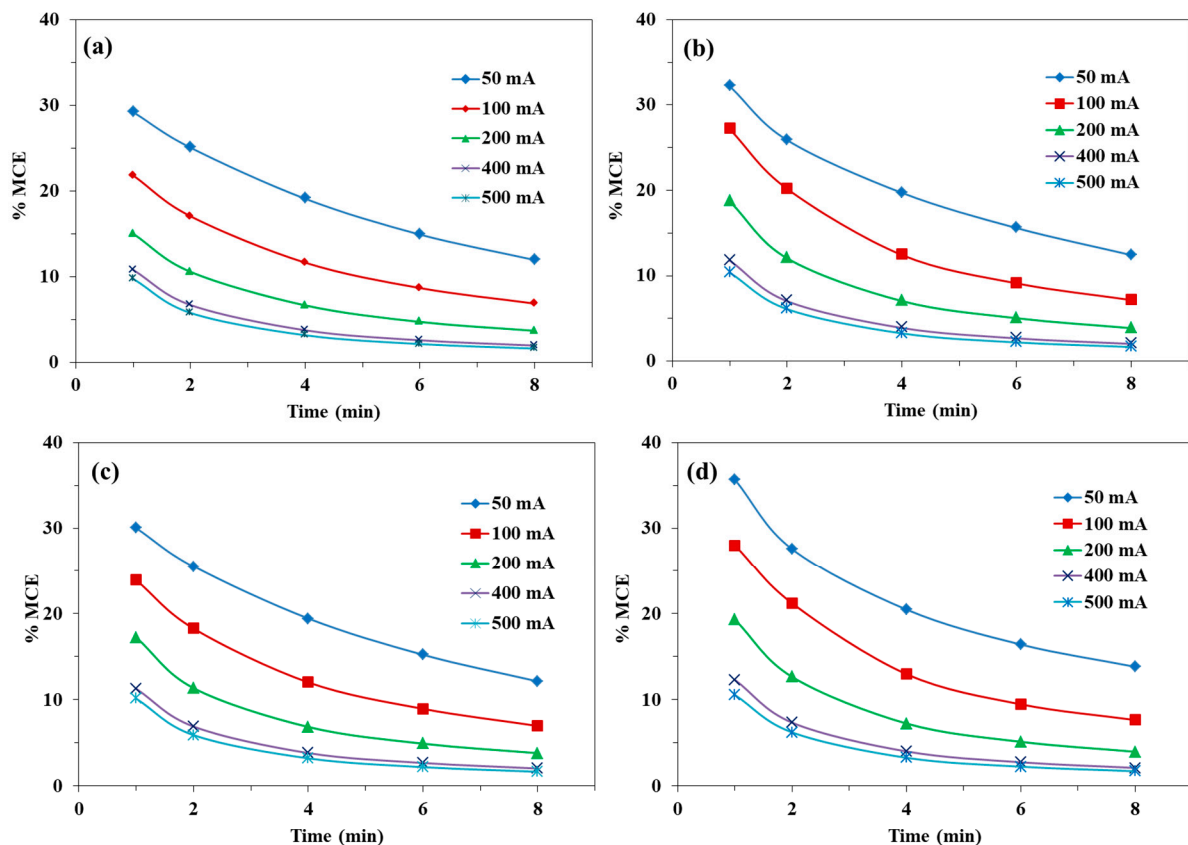


Figure 6. Effect of current on % mineralization current efficiency (MCE) in the heterogeneous electro-Fenton process (HEF) using different mineral iron-based catalysts: (a) ilmenite, (b) pyrite, (c) chromite, and (d) chalcopyrite.

However, MCE% decreased with longer electrolysis time in all cases. This trend is in agreement with previous reports [36,48,60,61] and can be related to the impoverishment of carbon matter in the medium and to the formation of persistent intermediates which are hardly mineralized such as short chain carboxylic acids. Moreover, increasing the current values led to a reduction in the MCE% values as a result of the energy loss through parasitic reactions consuming generated $\bullet\text{OH}$. The most important of these parasitic reactions include the wasting of $\bullet\text{OH}$ by Fe^{2+} (Equation (6)), recombination of $\bullet\text{OH}$ to H_2O_2 in the bulk (Equation (14)), oxidation of heterogeneous $\bullet\text{OH}$ at the BDD surface (Equation (15)) and electroreduction of H_2O_2 at the carbon felt (Equation (16)).



The amount of specific electrical energy consumed per TOC mass removed (SEC_{TOC}) is one of the important parameters for evaluating the energy for an electrochemical process from an industrial point of view. The values of SEC_{TOC} (in kWh per g TOC removed) in HEF with different natural catalysts are depicted in Figure 7. As these results show, an increase in applied current (between 50–500 mA) augments the electrical energy consumption regardless of the type of catalyst. In addition, the SEC_{TOC} values obviously increased with longer electrolysis times for all cases. For example, in the case of ilmenite, SEC_{TOC} is quite low (about $0.08 \text{ kWh (g TOC)}^{-1}$) in the early stage of treatment at 50 mA but it increased significantly (to about $0.22 \text{ kWh (g TOC)}^{-1}$) at the end of the electrochemical process. Besides, the SEC_{TOC} values are significantly high even at early treatment times ($0.40 \text{ kWh (g TOC)}^{-1}$ at 1 h) when applying high current (500 mA) and strongly increase over the electrolysis time ($2.58 \text{ kWh (g TOC)}^{-1}$) at 8 h. It can be inferred that the energy cost of working at 50 mA is 11.7 times lower than that of 500 mA at the end of the electrolysis, although it is important to note, as in Section 2.4, that higher applied currents lead to higher TOC removal efficiency. According to the results of Figure 7, among four iron-based natural catalysts, the chalcopyrite provides slightly better performance after 8 h electrolysis.

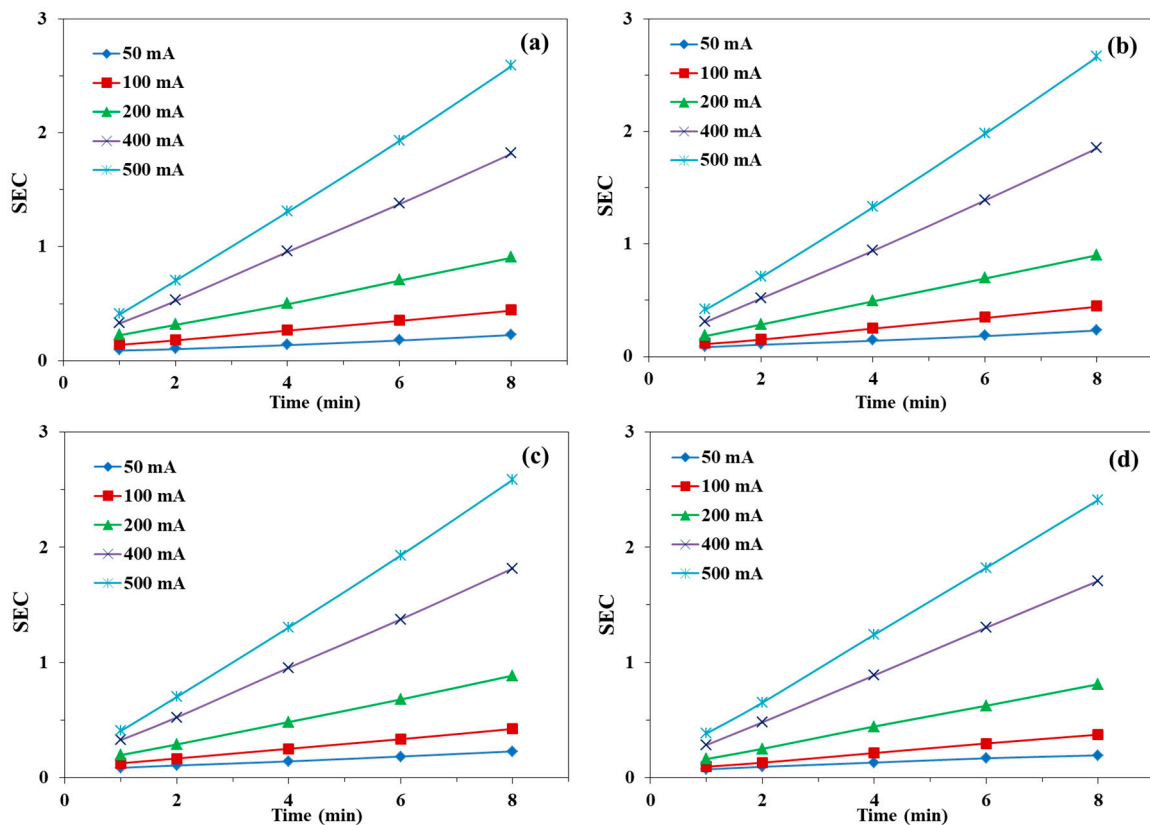


Figure 7. Effect of current and electrolysis time on specific energy consumption (SEC)_{TOC} during mineralization of 0.2 mM CFZ by HEF process using different mineral iron-based catalysts: (a) ilmenite, (b) pyrite, (c) chromite, and (d) chalcopyrite.

2.6. Stability and Reusability of the Catalysts

Stability and reusability are the main benefits of a heterogeneous catalyst compared to homogeneous catalysts, due to their easier separation from solution for reuse. Along with the catalytic activity, reusability is also important, because this can reduce the treatment cost. Therefore, this parameter was investigated under the same experimental conditions by five consecutive runs for chalcopyrite. After each run, and before the next experiment, the used chalcopyrite particles were collected from the experimental medium and washed several times with water to eliminate the impurities. The washed chalcopyrite particles

were dried in the oven (80 °C for 24 h). The results for CFZ degradation by HEF using chalcopyrite in five cycles are presented in Figure 8. As is obvious from these results, chalcopyrite presented significant chemical stability and only a negligible reduction (5%) was observed in the process efficiency after the fifth run. This very slight decrease in the catalytic activity of chalcopyrite can be due to catalyst poisoning by contaminant molecules, or the formation of intermediates and/or catalyst deactivation after five electrochemical cycles. These findings indicate the possibility of chalcopyrite for reuse and its application over a longer operation time.

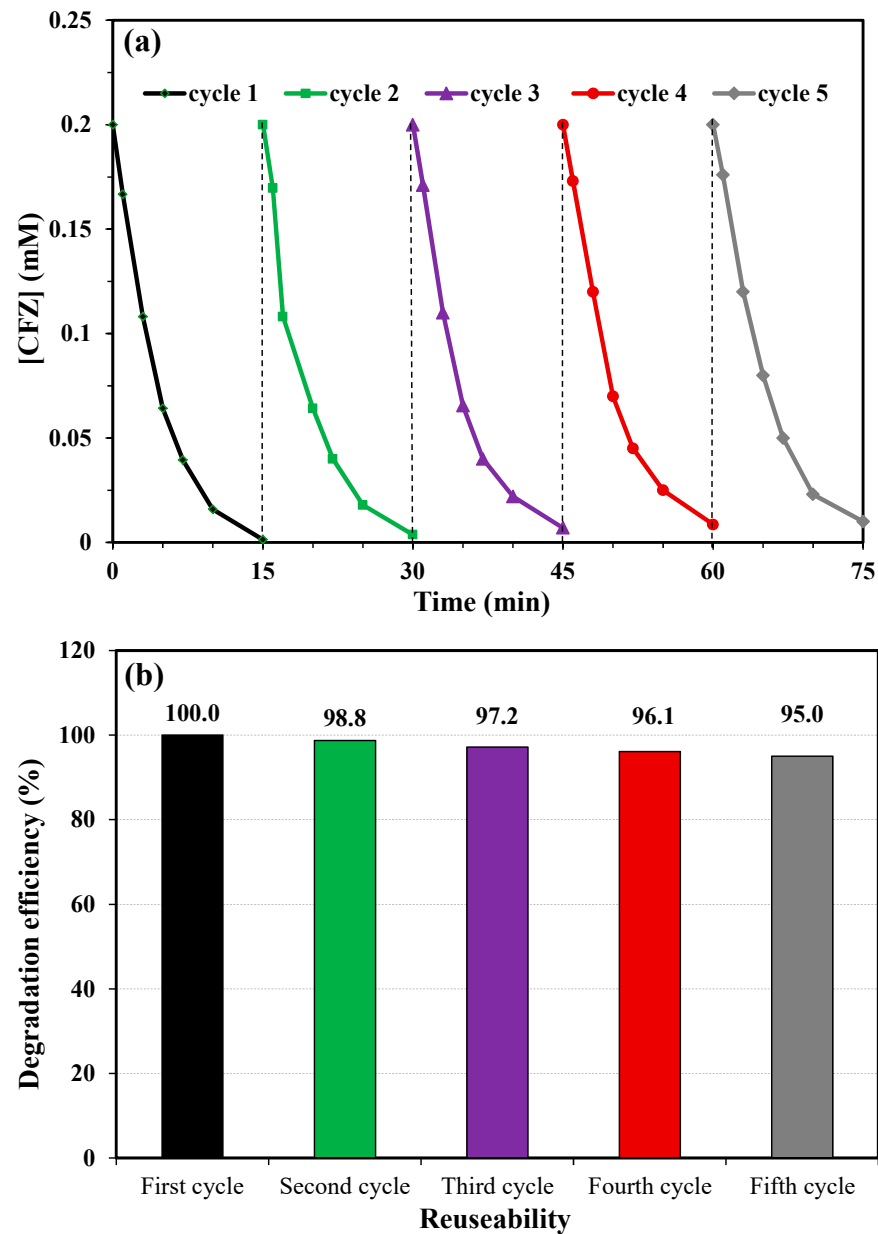


Figure 8. Stability for reusability of chalcopyrite in CFZ degradation during HEF within five consecutive cycles: Evolution of (a) catalytic activity and (b) Decay (%) in CFZ concentration.

2.7. Comparison of the Performance of the HEF Process Using Mineral Catalysts with other Processes for CFZ Degradation/Mineralization

This is the first study on the degradation of CFZ with the HEF process. Therefore, a literature review was carried out in order to compare the performance of the HEF process in degradation/mineralization of CFZ with already published reports (Table 2) on

the treatment of CFZ. This table summarizes the comparison between the current study and different other methods used for the degradation/mineralization of CFZ. As can be observed, the CFZ degradation by mineral iron-based HEF seems to be more efficient than that in other strategies. The obtained results highlight the potentiality of the low cost and available iron-based minerals to be used as catalysts for CFZ degradation/mineralization by the HEF process.

Table 2. Comparison of CFZ degradation/mineralization by HEF and other processes.

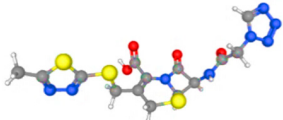
Method	Catalyst	Experimental Condition	Results	Ref.
Photocatalysis	TiO ₂	[CFZ] = 10 mM, [Cat] = 1.2 g L ⁻¹ , pH = 6.4	53% degradation in 60 min	[9]
Photocatalysis	N-doped TiO ₂	[CFZ] = 10 mM, [Cat] = 1.2 g L ⁻¹ , pH = 6.4	80% degradation in 30 min	[9]
Sono-catalysis	Ag ₃ PO ₄ /BiOBr composites	[CFZ] = 0.03 mM, [Cat] = 0.75 g L ⁻¹ , pH = 6.25	complete degradation in 30 min	[12]
Photocatalysis	TiO ₂	[CFZ] = 0.04 mM, [Cat] = 0.4 g L ⁻¹ , pH = 5, Light intensity = 17 W m ⁻²	86% COD removal in 120 min	[62]
Photocatalysis	ZnO/Activated carbon	[CFZ] = 0.2 mM, [Cat] = 100 mg L ⁻¹ , pH = 3	96% degradation in 60 min	[63]
Peroxy-mono-sulfate oxidation	CoFe ₂ O ₄ -rGO and PMS	[CFZ] = 0.04 mM, [Cat] = 0.1 g L ⁻¹ , [PMS] = 0.1 mM, pH = 6.5	almost complete degradation in 30 min	[64]
MnO ₂ oxidation	δ-MnO ₂	[CFZ] = 0.3 μM, [Cat] = 4 mg L ⁻¹ , pH = 4	20% degradation in 30 h	[65]
Heterogeneous electro-Fenton	Chalcopyrite	[CFZ] = 0.2 mM, [Cat] = 1 g L ⁻¹ , I = 200 mA, pH = 3	complete degradation in 15 min and almost complete mineralization in 8 h	This study
Heterogeneous electro-Fenton	Ilmenite Pyrite Chromite	[CFZ] = 0.2 mM, [Cat] = 1 g L ⁻¹ , I = 200 mA, pH = 3	complete degradation in 20 min and almost complete mineralization in 8 h	This study

3. Material and Methods

3.1. Materials

All chemical materials used in this research were in analytical grade and purchased from Fluka (Buchs, Switzerland), Merck (Darmstadt, Germany), and Acros Organics (Fair Lawn, New Jersey, United States). Sodium sulfate (Na₂SO₄) and sulfuric acid (H₂SO₄) were used as the electrolyte of the solution and the pH regulator, respectively. High purity CFZ (C₁₄H₁₄N₈O₄S₃) was obtained from Daana pharmaceutical company (Iran). The CFZ structure and chemical characteristic are shown in Table 3. All solutions were prepared by double-distilled water (Millipore Milli-Q) and experiments were performed at room temperature. Potassium hydrogen phthalate (C₈H₅KO₄, 99.5%) was used for calibration of TOC analyses. Natural mineral tuffs of ilmenite, chromite, pyrite and chalcopyrite were attained from the Moeil mine of Ardabil province (Iran) and used as heterogeneous catalysts in the HEF process. Natural iron-based tuffs were crushed and sieved to obtain fine particles with a size of approximately 270 μm by ball milling. To remove any unexpected impurities and water-soluble residues, the micro-grained natural samples were washed with ethanol and water. The procedure was followed by drying in the oven (343 K, 24 h). Then the mineral catalysts were ready to be used in HEF.

Table 3. Characteristic of the cefazolin.

Common Name	Chemical Formula	PubChem Substance ID	Chemical Structure	λ_{max} (nm)	CAS No.	MW (g/mol)
Cefazolin	C ₁₄ H ₁₄ N ₈ O ₄ S ₃	23675322		271	25953-19-9	476.5

3.2. Analysis Methods

The crystalline structures of mineral catalysts were evaluated by a Siemens X-ray diffraction (XRD, D5000, Munich, Germany) armed with a Cu K α (40 mA, 45 kV, and $\lambda = 1.5418 \text{ \AA}$). XRD analysis was performed in 2θ range of 10 to 80°. The molecular structure of the catalysts was characterized by using Raman spectroscopy (Takram P50C0R10) equipped with a diode light ($\lambda = 780 \text{ nm}$).

The time course of CFZ decay through oxidation was monitored by a reversed phase HPLC using a Merck Lachrom system (Hitachi, Darmstadt, Germany) equipped with an L-7100 quaternary pump and mounted by a Purospher RP 18 (5 μm , 25 cm \times 4.6 mm column at 40 °C) and an L-7455 photodiode array detector (Hitachi, Darmstadt, Germany), which was set to 270 nm. The analysis of CFZ was performed isocratically and the pH of the mobile phase was maintained at 6.8 by means of a phosphate buffer (a standard aqueous solution of K₂HPO₄, KH₂PO₄, and H₃PO₄). The mobile phase consisted of a mixture of phosphate buffer and methanol at volume ration of 70:30 with a flow rate of 0.8 mL min⁻¹. Mineralization of the CFZ solutions was assessed from the decrease of total organic carbon (TOC) which was evaluated by a Shimadzu analyzer (VCSH TOC, Shimadzu, Kyoto, Japan). The solution pH was adjusted with a CyberScan pH-meter (EuTech Instruments, Toronto, Canada) using H₂SO₄ or NaOH solutions.

3.3. Procedures of Heterogeneous Electro-Fenton Process

The electrolysis experiments were performed in an undivided and open cylindrical cell (250 mL) at room temperature. A 3D carbon-felt piece was used as cathode with dimensions of 15 cm \times 5 cm \times 0.5 cm and a thin-film BDD on Nb substrate (25 cm², Condias GmbH, Germany) was used as anode. The BDD anode was placed at the center of the cell while surrounded by the carbon felt cathode. The solution was subjected to vigorous stirring with a magnetic bar and continuously compressed air (1 L min⁻¹) was bubbled into the cell to maintain O₂ saturation. A schematic representation of the electrochemical experimental setup is shown in Figure 9. All comparative tests were carried out under the same operational conditions. Electrolysis was conducted with 0.2 mM CFZ in 0.05 M Na₂SO₄ solutions in presence of different amounts of natural iron-based catalysts (0.5–2 g L⁻¹), applying constant current between 50 and 500 mA by a Hameg HM8040 triple power supply (Mainhausen, Germany). The pH solution was regulated by sulfuric or hydrochloric acids to about 3 before starting the electrolysis. During the experiments, the samples were taken from the solution at different time intervals to evaluate the degradation rate and TOC removal efficiency using Equations (17) and (18), respectively.

$$\text{Degradation (\%)} = \frac{[C]_0 - [C]}{[C]_0} \times 100 \quad (17)$$

$$\text{TOC removal (\%)} = \left(\frac{\text{TOC}_0 - \text{TOC}}{\text{TOC}_0} \right) \times 100 \quad (18)$$

where (C)₀ and TOC₀ are CFZ concentration and solution TOC value of initial solution whereas (C) and TOC are CFZ concentration and solution TOC value at any time. The obtained TOC values were then used to calculate the mineralization rate of final CFZ

solution, the mineralization current efficiency (MCE) and specific energy consumption (SEC) from Equations (19) and (20), respectively:

$$\text{MCE}\% = \frac{nFV_s\Delta(\text{TOC})_{\text{exp}}}{4.32 \times 10^7 mIt} \times 100 \quad (19)$$

$$\text{SEC}_{\text{TOC}} \left(\text{kWhg}^{-1}\text{TOC} \right) = \frac{E_{\text{cell}}It}{V_s\Delta(\text{TOC})_{\text{exp}}} \quad (20)$$

where n , F and V_s are the number of electrons spent for CFZ mineralization, the Faraday constant (96485 C mol^{-1}) and the volume of solution (L), respectively. $\Delta(\text{TOC})_{\text{exp}}$ is the TOC decrease at time t (mg L^{-1}), 4.32×10^7 is a conversion coefficient for unit normalization, m is the number of carbon atoms of CFZ ($=14$), I is the applied current (A), t is reaction time (h) and E_{cell} is the cell voltage (V) developed between anode and cathode. The number of electrons (n) consumed for mineralization of the CFZ molecule was determined as 56 according to electrochemical mineralization reaction (Equation (21)), assuming the transformation of the organic nitrogen to ammonium ions during the mineralization process.

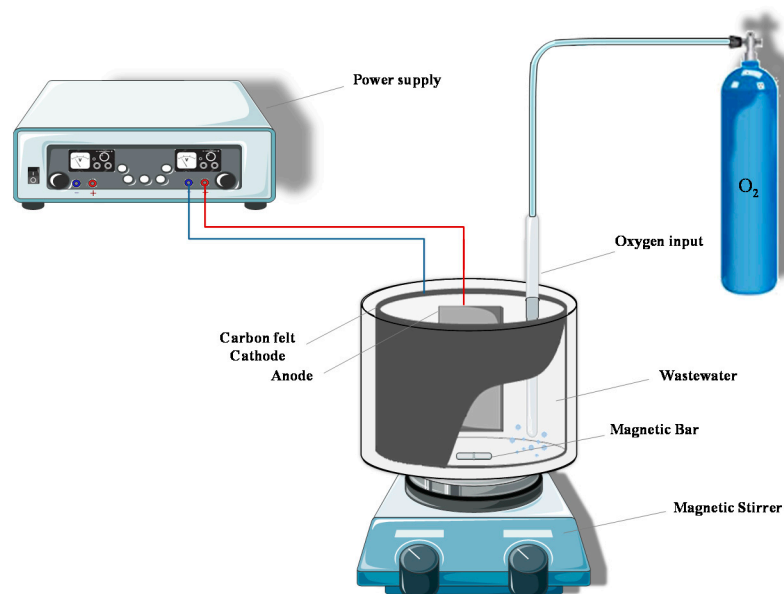


Figure 9. Schematic illustration of electrochemical setup used in this study.

4. Conclusions

Different iron-based natural catalysts, namely ilmenite, pyrite, chromite, and chalcopyrite, were used, as sustainable heterogeneous catalysts, in HEF. The chemical structures of iron-based catalysts were confirmed by XRD and Raman analyses. The catalytic activities of titled catalysts were comparatively evaluated for oxidation efficiency and mineralization rate during treatment of the antibiotic CFZ by HEF using BDD and carbon felt electrodes. These mineral catalysts can properly provide Fe^{2+} ions for generation of a powerful oxidant ($\bullet\text{OH}$) through the Fenton reaction. In all cases, the effect of the applied current, as one of the most significant operating parameters, was investigated on the degradation and mineralization of CFZ. Moreover, the amount of catalyst loading was investigated under the optimized current value of 200 mA. Results showed that the highest CFZ degradation efficiency was attained at 1 g L^{-1} for all mentioned mineral catalysts. The kinetic studies revealed that CFZ degradation by HEF follows the pseudo first-order kinetics. The chal-

copyrite presented the highest rate constant ($k_{app} = 0.241 \text{ min}^{-1}$ for $I = 200 \text{ mA}$) among different catalysts, which can be related to the presence of Cu^{2+} ions which catalyze the H_2O_2 decomposition in a Fenton like reaction to generate additional $\bullet\text{OH}$. The CFZ complete degradation in HEF using chalcopyrite occurred, comparatively, in a short reaction time at different currents, although the comparative performance of all mentioned catalysts showed very close ability for CFZ mineralization. Consequently, the MCE and energy consumption outcomes were almost similar for ilmenite, pyrite, chalcopyrite, and chromite catalysts after 8 h electrolysis. The excellent reusability and negligible reduction in catalytic activity of chalcopyrite catalyst in five consecutive runs highlights the practical applicability of this mineral catalyst for use in HEF to remove organic pollutants from wastewaters.

Author Contributions: Z.H.: Investigation, Writing, Formal analysis. R.P.: Conceptualization. R.A.: Editing, Reviewing. N.O.: Supervision, Review & editing, Methodology. S.S.: Draft preparation, Formal analysis, Reviewing. M.A.O.: Supervision, Validation, Review & editing, Project administration. All authors have read and agreed to the published version of the manuscript.

Funding: This research received no external funding.

Institutional Review Board Statement: Not applicable.

Informed Consent Statement: Not applicable.

Data Availability Statement: Data is contained within the article.

Acknowledgments: The authors acknowledge Gustave Eiffel University for providing financial and technical supports to perform this research. Also, S. Shirazian gratefully acknowledges the supports by the Government of the Russian Federation (Act 211, contract 02.A03.21.0011) and the Ministry of Science and Higher Education of the Russian Federation (grant FENU-2020-0019).

Conflicts of Interest: The authors declare no conflict of interest.

References

1. Brillas, E.; Martínez-Huitle, C.A. Decontamination of wastewaters containing synthetic organic dyes by electrochemical methods. An updated review. *Appl. Catal. B Environ.* **2015**, *166*, 603–643. [[CrossRef](#)]
2. García-Montoya, M.F.; Gutierrez-Granados, S.; Alatorre-Ordaz, A.; Galindo, R.; Ornelas, R.; Peralta-Hernandez, J.M. Application of electrochemical/BDD process for the treatment wastewater effluents containing pharmaceutical compounds. *J. Ind. Eng. Chem.* **2015**, *31*, 238–243. [[CrossRef](#)]
3. Jain, B.; Singh, A.K.; Kim, H.; Lichtfouse, E.; Sharma, V.K. Treatment of organic pollutants by homogeneous and heterogeneous Fenton reaction processes. *Environ. Chem. Lett.* **2018**, *16*, 947–967. [[CrossRef](#)]
4. Rodrigo, M.; Oturan, N.; Oturan, M.A. Electrochemically assisted remediation of pesticides in soils and water: A review. *Chem. Rev.* **2014**, *114*, 8720–8745. [[CrossRef](#)]
5. Mompelat, S.; Le Bot, B.; Thomas, O. Occurrence and fate of pharmaceutical products and by-products, from resource to drinking water. *Environ. Int.* **2009**, *35*, 803–814. [[CrossRef](#)]
6. Besse, J.-P.; Kausch-Barreto, C.; Garric, J. Exposure assessment of pharmaceuticals and their metabolites in the aquatic environment: Application to the French situation and preliminary prioritization. *Hum. Ecol. Risk Assess.* **2008**, *14*, 665–695. [[CrossRef](#)]
7. Gros, M.; Petrović, M.; Barceló, D. Wastewater treatment plants as a pathway for aquatic contamination by pharmaceuticals in the Ebro river basin (northeast Spain). *Environ. Toxicol. Chem. Int. J.* **2007**, *26*, 1553–1562. [[CrossRef](#)]
8. Wei, R.; Ge, F.; Huang, S.; Chen, M.; Wang, R. Occurrence of veterinary antibiotics in animal wastewater and surface water around farms in Jiangsu Province, China. *Chemosphere* **2011**, *82*, 1408–1414. [[CrossRef](#)]
9. Gurkan, Y.Y.; Turkten, N.; Hatipoglu, A.; Cinar, Z. Photocatalytic degradation of cefazolin over N-doped TiO_2 under UV and sunlight irradiation: Prediction of the reaction paths via conceptual DFT. *Chem. Eng. J.* **2012**, *184*, 113–124. [[CrossRef](#)]
10. Rechelo, B.S.; Kogawa, A.C.; Salgado, H.R.N. Quantitative analysis of cefazolin sodium in lyophilized powder by infrared spectrophotometry: Green, low cost, fast and effective. *Spectrochim. Acta Part A Mol. Biomol. Spectrosc.* **2019**, *208*, 157–161. [[CrossRef](#)]
11. Ikehata, K.; Naghashkar, N.J.; El-Din, M.G. Degradation of aqueous pharmaceuticals by ozonation and advanced oxidation processes: A review. *Ozone Sci. Eng.* **2006**, *28*, 353–414. [[CrossRef](#)]
12. Xiao, Y.; Song, X.; Liu, Z.; Li, R.; Zhao, X.; Huang, Y. Photocatalytic removal of cefazolin using $\text{Ag}_3\text{PO}_4/\text{BiOBr}$ under visible light and optimization of parameters by response surface methodology. *J. Ind. Eng. Chem.* **2017**, *45*, 248–256. [[CrossRef](#)]
13. Li, L.; Wei, D.; Wei, G.; Du, Y. Transformation of cefazolin during chlorination process: Products, mechanism and genotoxicity assessment. *J. Hazard. Mater.* **2013**, *262*, 48–54. [[CrossRef](#)] [[PubMed](#)]

14. Stackelberg, P.E.; Gibs, J.; Furlong, E.T.; Meyer, M.T.; Zaugg, S.D.; Lippincott, R.L. Efficiency of conventional drinking-water-treatment processes in removal of pharmaceuticals and other organic compounds. *Sci. Total Environ.* **2007**, *377*, 255–272. [[CrossRef](#)] [[PubMed](#)]
15. Simazaki, D.; Kubota, R.; Suzuki, T.; Akiba, M.; Nishimura, T.; Kunikane, S. Occurrence of selected pharmaceuticals at drinking water purification plants in Japan and implications for human health. *Water Res.* **2015**, *76*, 187–200. [[CrossRef](#)] [[PubMed](#)]
16. Carmona, E.; Andreu, V.; Picó, Y. Occurrence of acidic pharmaceuticals and personal care products in Turia River Basin: From waste to drinking water. *Sci. Total Environ.* **2014**, *484*, 53–63. [[CrossRef](#)]
17. Wieszczycka, K.; Filipowiak, K.; Wojciechowska, I.; Aksamitowski, P. Novel ionic liquid-modified polymers for highly effective adsorption of heavy metals ions. *Separation Purif. Technol.* **2020**, *236*, 116313. [[CrossRef](#)]
18. Gibson, L. Mesosilica materials and organic pollutant adsorption: Part B removal from aqueous solution. *Chem. Soc. Rev.* **2014**, *43*, 5173–5182. [[CrossRef](#)]
19. Pelalak, R.; Soltani, R.; Heidari, Z.; Malekshah, R.E.; Aallaei, M.; Marjani, A.; Rezakazemi, M.; Kurniawan, T.A.; Shirazian, S. Molecular dynamics simulation of novel diamino-functionalized hollow mesosilica spheres for adsorption of dyes from synthetic wastewater. *J. Mol. Liq.* **2020**, *322*, 114812. [[CrossRef](#)]
20. Soltani, R.; Pelalak, R.; Pishnamazi, M.; Marjani, A.; Shirazian, S. Synthesis of Multi-organo-functionalized Fibrous silica KCC-1 for Highly Efficient Adsorption of Acid Fuchsin and acid Orange II from Aqueous Solution. *Sci. Rep.* **2020**. [[CrossRef](#)]
21. Soltani, R.; Pishnamazi, M.; Pelalak, R.; Rezakazemi, M.; Marjani, A.; Dinari, M.; Sarkar, S.M.; Shirazian, S. Preparation of COOH-KCC-1/polyamide 6 composite by in situ ring-opening polymerization: Synthesis, characterization, and Cd(II) adsorption study. *J. Environ. Chem. Eng.* **2020**, 104683. [[CrossRef](#)]
22. Pelalak, R.; Heidari, Z.; Soltani, H.; Shirazian, S. Mathematical model for numerical simulation of organic compound recovery using membrane separation. *Chem. Eng. Technol.* **2018**, *41*, 345–352. [[CrossRef](#)]
23. Soltani, H.; Pelalak, R.; Heidari, Z.; Ghadiri, M.; Shirazian, S. CFD simulation of transport phenomena in wastewater treatment via vacuum membrane distillation. *J. Porous Media* **2016**, *19*, 515–526. [[CrossRef](#)]
24. Nguyen, P.; Carvalho, G.; Reis, M.A.; Oehmen, A. A review of the biotransformations of priority pharmaceuticals in biological wastewater treatment processes. *Water Res.* **2020**, *188*, 116446. [[CrossRef](#)] [[PubMed](#)]
25. Tiwari, B.; Sellamuthu, B.; Ouarda, Y.; Drogui, P.; Tyagi, R.D.; Buelna, G. Review on fate and mechanism of removal of pharmaceutical pollutants from wastewater using biological approach. *Bioresour. Technol.* **2017**, *224*, 1–12. [[CrossRef](#)] [[PubMed](#)]
26. Heidari, Z.; Alizadeh, R.; Ebadi, A.; Pelalak, R.; Oturan, N.; Oturan, M.A. Degradation of furosemide using photocatalytic ozonation in the presence of ZnO/ICLT nanocomposite particles: Experimental, modeling, optimization and mechanism evaluation. *J. Mol. Liq.* **2020**, *319*, 114193. [[CrossRef](#)]
27. Rosal, R.; Rodríguez, A.; Perdigón-Melón, J.; Mezcuca, M.; Hernando, M.; Letón, P.; García-Calvo, E.; Agüera, A.; Fernández-Alba, A. Removal of pharmaceuticals and kinetics of mineralization by O₃/H₂O₂ in a biotreated municipal wastewater. *Water Res.* **2008**, *42*, 3719–3728. [[CrossRef](#)]
28. Pelalak, R.; Alizadeh, R.; Ghareshabani, E. Enhanced heterogeneous catalytic ozonation of pharmaceutical pollutants using a novel nanostructure of iron-based mineral prepared via plasma technology: A comparative study. *J. Hazard. Mater.* **2020**, *392*, 122269. [[CrossRef](#)]
29. Oturan, M.A.; Aaron, J.-J. Advanced Oxidation Processes in Water/Wastewater Treatment: Principles and Applications. A Review. *Crit. Rev. Environ. Sci. Technol.* **2014**, *44*, 2577–2641. [[CrossRef](#)]
30. Giwa, A.; Yusuf, A.; Balogun, H.A.; Sambudi, N.S.; Bilad, M.R.; Adeyemi, I.; Chakraborty, S.; Curcio, S. Recent advances in advanced oxidation processes for removal of contaminants from water: A comprehensive review. *Process Saf. Environ. Prot.* **2020**, *146*, 220–256. [[CrossRef](#)]
31. Tufail, A.; Price, W.E.; Mohseni, M.; Pramanik, B.K.; Hai, F.I. A critical review of advanced oxidation processes for emerging trace organic contaminant degradation: Mechanisms, factors, degradation products, and effluent toxicity. *J. Water Process Eng.* **2020**, 101778. [[CrossRef](#)]
32. Heidari, Z.; Alizadeh, R.; Ebadi, A.; Oturan, N.; Oturan, M.A. Efficient photocatalytic degradation of furosemide by a novel sonoprecipitated ZnO over ion exchanged clinoptilolite nanorods. *Sep. Purif. Technol.* **2020**, *242*, 116800. [[CrossRef](#)]
33. Pelalak, R.; Alizadeh, R.; Ghareshabani, E.; Heidari, Z. Degradation of sulfonamide antibiotics using ozone-based advanced oxidation process: Experimental, modeling, transformation mechanism and DFT study. *Sci. Total Environ.* **2020**, *734*, 139446. [[CrossRef](#)] [[PubMed](#)]
34. Casado, J. Towards industrial implementation of Electro-Fenton and derived technologies for wastewater treatment: A review. *J. Environ. Chem. Eng.* **2019**, *7*, 102823. [[CrossRef](#)]
35. Chaplin, B.P. Critical review of electrochemical advanced oxidation processes for water treatment applications. *Environ. Sci. Process. Impacts* **2014**, *16*, 1182–1203. [[CrossRef](#)] [[PubMed](#)]
36. Brillas, E.; Sirés, I.; Oturan, M.A. Electro-Fenton Process and Related Electrochemical Technologies Based on Fenton's Reaction Chemistry. *Chem. Rev.* **2009**, *109*, 6570–6631. [[CrossRef](#)]
37. Zhou, M.; Oturan, M.A.; Sires, I. *Electro-Fenton Process*; Springer: Berlin, Germany, 2018.
38. Barhoumi, N.; Oturan, N.; Olvera-Vargas, H.; Brillas, E.; Gadri, A.; Ammar, S.; Oturan, M.A. Pyrite as a sustainable catalyst in electro-Fenton process for improving oxidation of sulfamethazine. Kinetics, mechanism and toxicity assessment. *Water Res.* **2016**, *94*, 52–61. [[CrossRef](#)]

39. Ammar, S.; Oturan, M.A.; Labiadh, L.; Guersalli, A.; Abdelhedi, R.; Oturan, N.; Brillas, E. Degradation of tyrosol by a novel electro-Fenton process using pyrite as heterogeneous source of iron catalyst. *Water Res.* **2015**, *74*, 77–87. [[CrossRef](#)]
40. Ganiyu, S.O.; Martínez-Huitle, C.A. Nature, Mechanisms and Reactivity of Electrogenerated Reactive Species at Thin-Film Boron-Doped Diamond (BDD) Electrodes During Electrochemical Wastewater Treatment. *ChemElectroChem* **2019**, *6*, 2379–2392. [[CrossRef](#)]
41. Nidheesh, P.; Divyapriya, G.; Oturan, N.; Trelu, C.; Oturan, M.A. Environmental applications of boron-doped diamond electrodes: 1. Applications in water and wastewater treatment. *ChemElectroChem* **2019**, *6*, 2124–2142. [[CrossRef](#)]
42. Weiss, E.; Groenen-Serrano, K.; Savall, A. Electrochemical mineralization of sodium dodecylbenzenesulfonate at boron doped diamond anodes. *J. Appl. Electrochem.* **2007**, *37*, 1337–1344. [[CrossRef](#)]
43. Panizza, M.; Cerisola, G. Application of diamond electrodes to electrochemical processes. *Electrochim. Acta* **2005**, *51*, 191–199. [[CrossRef](#)]
44. Ganiyu, S.O.; Zhou, M.; Martínez-Huitle, C.A. Heterogeneous electro-Fenton and photoelectro-Fenton processes: A critical review of fundamental principles and application for water/wastewater treatment. *Appl. Catal. B Environ.* **2018**, *235*, 103–129. [[CrossRef](#)]
45. Poza-Nogueiras, V.; Rosales, E.; Pazos, M.; Sanromán, M. Current advances and trends in electro-Fenton process using heterogeneous catalysts—A review. *Chemosphere* **2018**, *201*, 399–416. [[CrossRef](#)]
46. Nidheesh, P.V. Heterogeneous Fenton catalysts for the abatement of organic pollutants from aqueous solution: A review. *RSC Adv.* **2015**, *5*, 40552–40577. [[CrossRef](#)]
47. Thomas, N.; Dionysiou, D.D.; Pillai, S.C. Heterogeneous Fenton catalysts: A review of recent advances. *J. Hazard. Mater.* **2021**, *404*, 124082. [[CrossRef](#)]
48. Barhoumi, N.; Labiadh, L.; Oturan, M.A.; Oturan, N.; Gadri, A.; Ammar, S.; Brillas, E. Electrochemical mineralization of the antibiotic levofloxacin by electro-Fenton-pyrite process. *Chemosphere* **2015**, *141*, 250–257. [[CrossRef](#)]
49. Expósito, E.; Sánchez-Sánchez, C.M.; Montiel, V. Mineral Iron Oxides as Iron Source in Electro-Fenton and Photoelectro-Fenton Mineralization Processes. *J. Electrochem. Soc.* **2007**, *154*, 116–122. [[CrossRef](#)]
50. Fang, G.-D.; Dionysiou, D.D.; Al-Abed, S.R.; Dong-Mei, Z. Superoxide radical driving the activation of persulfate by magnetite nanoparticles: Implications for the degradation of PCBs. *Appl. Catal. B Environ.* **2013**, *129*, 325–332. [[CrossRef](#)]
51. Silveira, J.E.; Zazo, J.A.; Pliego, G.; Casas, J.A. Landfill leachate treatment by sequential combination of activated persulfate and Fenton oxidation. *Waste Manag.* **2018**, *81*, 220–225. [[CrossRef](#)]
52. Barhoumi, N.; Olvera-Vargas, H.; Oturan, N.; Huguenot, D.; Gadri, A.; Ammar, S.; Brillas, E.; Oturan, M.A. Kinetics of oxidative degradation/mineralization pathways of the antibiotic tetracycline by the novel heterogeneous electro-Fenton process with solid catalyst chalcopyrite. *Appl. Catal. B Environ.* **2017**, *209*, 637–647. [[CrossRef](#)]
53. Pataquiva-Mateus, A.Y.; Zea, H.R.; Ramirez, J.H. Degradation of Orange II by Fenton reaction using ilmenite as catalyst. *Environ. Sci. Pollut. Res.* **2017**, *24*, 6187–6194. [[CrossRef](#)] [[PubMed](#)]
54. Pelalak, R.; Baniadam, M.; Maghrebi, M. Controllable purification, cutting and unzipping of multi-walled carbon nanotubes with a microwave method. *Appl. Phys. A* **2013**, *111*, 951–957. [[CrossRef](#)]
55. Wu, X.; Qin, S.; Dubrovinsky, L. Structural characterization of the FeTiO₃–MnTiO₃ solid solution. *J. Solid State Chem.* **2010**, *183*, 2483–2489. [[CrossRef](#)]
56. Saavedra, A.; García-Meza, J.V.; Cortón, E.; González, I. Attachment of *Leptospirillum* sp. to chemically modified pyrite surfaces. Fast and simple electrochemical monitoring of bacterial-mineral interactions. *Hydrometallurgy* **2020**, *199*, 105534.
57. Sarkar, S.; Kumar, T.N.; Ray, D.; Bhattacharya, S.; Shukla, A.D.; Moitra, H.; Dagar, A.; Chauhan, P.; Sen, K.; Das, S. Mineralogy and spectroscopy (VIS near infrared and micro-Raman) of chromite from Nidar ophiolite complex, SE Ladakh, India: Implications for future planetary exploration. *Planet. Space Sci.* **2019**, *165*, 1–9.
58. Yang, B.; Yan, H.; Zeng, M.; Huang, P.; Jia, F.; Teng, A. A novel copper depressant for selective flotation of chalcopyrite and molybdenite. *Miner. Eng.* **2020**, *151*, 106309. [[CrossRef](#)]
59. Garcia-Segura, S.; Brillas, E.; Cornejo-Ponce, L.; Salazar, R. Effect of the Fe³⁺/Cu²⁺ ratio on the removal of the recalcitrant oxalic and oxamic acids by electro-Fenton and solar photoelectro-Fenton. *Sol. Energy* **2016**, *124*, 242–253. [[CrossRef](#)]
60. Zazou, H.; Oturan, N.; Sönmez Çelebi, M.; Hamdani, M.; Oturan, M.A. Cold incineration of 1,2-dichlorobenzene in aqueous solution by electrochemical advanced oxidation using DSA/Carbon felt, Pt/Carbon felt and BDD/Carbon felt cells. *Sep. Purif. Technol.* **2019**, *208*, 184–193. [[CrossRef](#)]
61. Oturan, N.; Ganiyu, S.O.; Raffy, S.; Oturan, M.A. Sub-stoichiometric titanium oxide as a new anode material for electro-Fenton process: Application to electrocatalytic destruction of antibiotic amoxicillin. *Appl. Catal. B Environ.* **2017**, *217*, 214–223. [[CrossRef](#)]
62. Shokri, M.; Isapour, G.; Behnajady, M.A.; Dorosti, S. A comparative study of photocatalytic degradation of the antibiotic cefazolin by suspended and immobilized TiO₂ nanoparticles. *Desalination Water Treat.* **2016**, *57*, 12874–12881. [[CrossRef](#)]
63. Samarghandi, M.; Rahmani, A.; Asgari, G.; Ahmadidoost, G.; Dargahi, A. Photocatalytic removal of cefazolin from aqueous solution by AC prepared from mango seed+ ZnO under uv irradiation. *Glob. Nest J.* **2018**, *20*, 399–407.
64. Fan, Y.; Zhou, Z.; Feng, Y.; Zhou, Y.; Wen, L.; Shih, K. Degradation mechanisms of ofloxacin and cefazolin using peroxymonosulfate activated by reduced graphene oxide-CoFe₂O₄ composites. *Chem. Eng. J.* **2020**, *383*, 123056. [[CrossRef](#)]
65. Hsu, M.H.; Kuo, T.H.; Chen, Y.E.; Huang, C.H.; Hsu, C.C.; Lin, A.Y.C. Substructure Reactivity Affecting the Manganese Dioxide Oxidation of Cephalosporins. *Environ. Sci. Technol.* **2018**, *52*, 9188–9195. [[CrossRef](#)]